Rapid Communications

Antiferromagnetic metallic state as proved by magnetotransport in epitaxially stabilized perovskite $PbRuO_3$

T. C. Fujita,[1,*] L. F. Zhang,[1] and M. Kawasaki[1,2]

[1]*Department of Applied Physics and Quantum Phase Electronics Center, University of Tokyo, Tokyo 113-8656, Japan*

[2]*RIKEN Center for Emergent Matter Science (CEMS), Wako 351-0198, Japan*

(Received 7 January 2020; revised manuscript received 27 February 2020; accepted 10 March 2020; published 23 March 2020)

Perovskite $PbRuO_3$, which has been synthesized only in bulk polycrystalline form under high pressure, is an orthorhombic *Pbnm* at room temperature, exhibiting structural phase transition to *Imma* at around 90 K. This structural transition is accompanied with an orbital ordering and antiferromagnetic spin fluctuation. Here, we report the fabrication of single crystalline perovskite $PbRuO_3$ thin films on various substrates. Magnetotransport measurements reveal that the films have metallic electronic ground state without any clear electronic transitions reported in previous literature. Evidenced by a shift of transition temperature, suppression of magnetic spin fluctuation due to epitaxial strain is implicated. Nonlinear Hall effect is also observed with indiscernible hysteresis, plausibly originating from antiferromagnetic spins, yet multiband effect cannot be completely ruled out.

DOI: 10.1103/PhysRevMaterials.4.031401

Transition metal oxide perovskites (ABO_3) are important materials practically used as components in electronic devices and also display a wide range of electronic phenomena such as superconductivity, colossal magnetoresistances, and multiferroicity as a result of coupled charge, orbital, and spin orderings [1,2]. Also in the past several decades, intensive efforts have been made to explore novel functionalities and emergent phenomena in heterostructures composed of transition metal oxides [3]. Among them, perovskite ruthenates (B = Ru) have been studied especially in terms of their metallicity originating from extended broad Ru-4*d* bands to elucidate correlated itinerant electron physics. All of the pseudocubic $ARuO_3$ perovskites (A = Ca, Sr, Ba) are metallic to the lowest measured temperatures, while their magnetic properties are largely dependent on A-site. $SrRuO_3$ and $BaRuO_3$ are ferromagnets with Curie temperatures (T_C) of 160 and 60 K, respectively [4–7], while $CaRuO_3$ does not show a magnetic transition [8]. Different from the rare-earth R^{3+} substitution in perovskite systems such as nickelates [9], the effect on electronic phase in $ARuO_3$ family cannot be simply predicted from the ionic radius because the substitution induces a significant change in chemistry as well as the size variance [10]. Indeed, the maximum T_C is found at $SrRuO_3$, and any Ca^{2+} or Ba^{2+} substitution for Sr^{2+} results in a reduction of T_C although metallic phase remains to the lowest temperature in this system. In this sense, $PbRuO_3$ (A = Pb) is an interesting compound since Pb^{2+} (1.49 Å) ionic radius locates in between those of Sr^{2+} (1.44 Å) and Ba^{2+} (1.61 Å). Additionally, Pb^{2+} sometimes causes further lattice distortion through "lone pair effect," which can introduce ferroelectricity in such compounds as $PbTiO_3$.

The perovskite $PbRuO_3$ was first synthesized under 9 GPa and 1400 °C in 1970 [11], but its low-temperature crystal structure and physical properties were not characterized until a recent report from Kimber *et al.* in 2009 [12]. They have revealed that $PbRuO_3$ undergoes a first-order structural transition from the *Pbnm* phase to the *Imma* phase on cooling at about 90 K. The local structural distortions resolved from a neutron diffraction study suggested an orbital ordering on Ru in the low temperature *Imma* phase. This structural phase transition was reported to be concomitant with an electronic phase transition from metal to insulator. Furthermore, $PbRuO_3$ has no long-range magnetic order down to 1.5 K while the presence of antiferromagnetic (AFM) spin fluctuation is suggested by a kink structure in the temperature dependence of magnetic susceptibility. These observations would be surprising because one can naively predict that the perovskite $PbRuO_3$ is a ferromagnetic metal by taking into account the aforementioned Pb^{2+} size. They attributed this drastic change in the electronic ground state to a possible orbital order and a hybridization between Pb-6*s* and Ru-4*d* electrons, which are also supported by their first-principles calculation in the same report. Soon after their report, J.-G. Cheng *et al.* have questioned the insulating ground state with no magnetic order of $PbRuO_3$ and have shown that $PbRuO_3$ exhibits structural phase transition accompanied with *metal-metal* transition at around 90 K [13], which is totally different from the previous report by Kimber *et al.* They have highlighted the uniqueness of the structural phase transition in this system by measuring properties under pressure; in contrast to ordinary perovskite oxides, *Imma* phase of $PbRuO_3$ is favorable at lower temperature and suppressed by pressure. Moreover, in later report, they have clarified another crystal phase transition from *Pbnm* to polar $Pbn2_1$ above a critical pressure around 32 GPa [14]. Later, A. F. Kusmartseva *et al.*

*Corresponding author: fujita@ap.t.u-tokyo.ac.jp

have explored quantum criticality of $PbRuO_3$ under high pressure and clarified that the observed metal-insulator transition by Kimber *et al.* was an artifact due to the breaking of intergrain connection at the structural transition [15]. They have found the suppression of the transition temperature towards zero at 5 GPa concomitant with an emergence of non-Fermi liquid behavior in resistivity and the presence of more resistive phase at 30 GPa and ambient temperature.

As introduced above, regardless of numbers of intriguing physical phenomena, magnetotransport properties have not been reported in $PbRuO_3$ because of the difficulty in synthesizing single crystal. With using considerable size of single crystalline thin films, well-defined Hall-bar device structure can be fabricated in order to clarify the magnetotransport properties. Also, in thin films, we have the possibility to control the physical properties of $PbRuO_3$ by epitaxial strain, because phase transition in bulk is seemingly affected by pressure [13–15]. Our transport studies for thin films reveal a metallic ground state of $PbRuO_3$ and emergence of nonlinear Hall effect, although any clear signature of the crystal phase transition has not been observed.

Single crystalline $PbRuO_3$ thin films were prepared on various substrates by pulsed laser deposition (PLD). The target was prepared in ambient by the solid-state reaction of PbO and RuO_2 at 1100 °C in stoichiometric proportions, resulting in single phase pyrochlore $Pb_2Ru_2O_{6.5}$. Although perovskite $PbRuO_3$ is a metastable phase and cannot be obtained by a simple solid state reaction at ambient pressure, we succeeded in fabrication of single crystalline thin films starting from the pyrochlore $Pb_2Ru_2O_{6.5}$ target after optimizing growth conditions. First, a series of films were deposited on $SrTiO_3$ (001) substrate to optimize growth conditions. A KrF laser with a pulse frequency of 5 Hz and fluence of ≈2 J/cm^2 was employed while changing the growth temperature and oxygen partial pressure. $SrTiO_3$ substrate was annealed *in situ* at 900 °C under 10^{-5} Torr O_2 to obtain clear step-terrace structure with single-unit-cell height. General temperature-pressure phase diagram is shown in Fig. 1, which can be classified into five regions based on x-ray diffraction. At high temperature and high oxygen partial pressure (region A), no film is obtained probably because precursors are re-evaporated as volatile RuO_3 and PbO. At high oxygen partial pressure but lower temperature (region B), PbO_x is formed. On the other hand, at lower oxygen partial pressure but high temperature (region C), RuO_2 is formed. When both temperature and oxygen partial pressure are low (region D), we cannot observe any x-ray diffraction peaks although we can see some film is deposited on the substrate, indicating that precursors form amorphous film due to the lack of formation energy. In the intermediate region (region E), both $Pb_2Ru_2O_{6.5}$ and targeted perovskite $PbRuO_3$ phases appear. Second, within the region E, in order to suppress the formation of $Pb_2Ru_2O_{6.5}$ phase, we reduce the laser frequency to slow down the growth rate. Finally, we reach the optimum growth conditions, and films are deposited on various substrates at 450 °C under 0.1 m Torr O_2 with a pulse frequency of 1 Hz and fluence of ≈2 J/cm^2, where typical growth rate is ≈0.01 Å/sec.

Having established the optimum growth conditions, we employed $(LaAlO_3)_{0.3}$ $(SrAl_{0.5}$ $Ta_{0.5}$ $O_3)_{0.7}$ (LSAT) (001) (cubic, 3.867 Å), $SrTiO_3$ (STO) (001) (cubic, 3.905 Å), $DyScO_3$ (DSO) (110) (orthorhombic, 3.942 Å in pseudocubic setting), and $GdScO_3$ (GSO) (110) (orthorhombic, 3.967 Å in pseudocubic setting). Bulk $PbRuO_3$ has orthorhombic crystal structure with $a = 5.563$ Å, $b = 5.614$ Å, and $c = 7.865$ Å, thus it can be seen as a pseudocubic structure with $a_{pc} = 3.945$ Å. Therefore, $PbRuO_3$ is subjected to compressive strains of −1.98, −1.02, and −0.07% on LSAT, STO, and DSO, and tensile strains of +0.39% on GSO, respectively. In prior to the growth on LSAT, DSO, and GSO substrates, 2 nm STO buffer layer was deposited at 600 °C under 0.1 m Torr O_2 environment, in order to ensure smoother surface and to relieve the valence discontinuity between these substrates with $PbRuO_3$, which is often crucial to obtain thermodynamically unstable compounds such as $SrMoO_3$ [16] and $EuMoO_3$ [17,18]. Electric conductivity of the STO buffer layer was examined to reveal that STO grown under the same condition was insulating. Thickness of the $PbRuO_3$ films were around 10 nm for LSAT, DSO and GSO samples, and around 5 nm for STO sample, which were confirmed by x-ray reflectivity measurements. The magnetotransport properties were obtained using a liquid He cryostat equipped with a 9 T superconducting magnet (PPMS, Quantum Design Co.). Magnetic field is applied perpendicular to the films. Longitudinal (ρ_{xx}) and Hall resistivity (ρ_H) are deduced by a conventional symmetrization and antisymmetrization procedures, respectively.

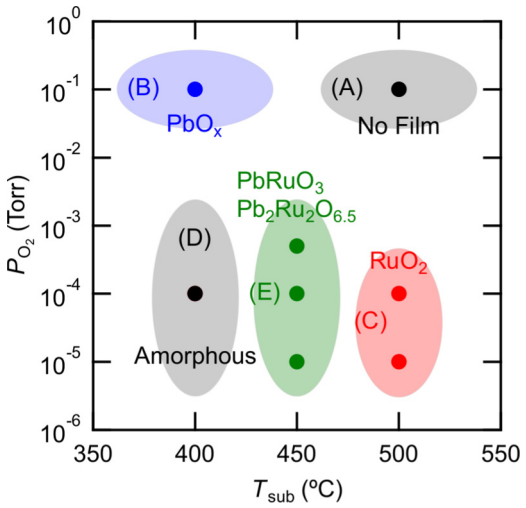

FIG. 1. Growth phase diagram of $PbRuO_3$ thin films. Depending on the growth temperature (T_{sub}) and oxygen partial pressure (P_{O_2}), the diagram classifies following five regions. (A) both Pb and Ru are evaporated. (B) Ru evaporates as volatile RuO_3 and only PbO_x remains. (C) Pb evaporates as volatile PbO and only RuO_2 remains. (D) Both Ru and Pb are in amorphous phase. (E) Coexistence region of stable $Pb_2Ru_2O_{6.5}$ and metastable $PbRuO_3$ phases.

X-ray diffraction (XRD) 2θ-ω scans and magnified XRD patterns around (002) (pseudocubic setting) peak of $PbRuO_3$ films are presented in Figs. 2(a) and 2(b). The (002) peaks of $PbRuO_3$ are indicated by triangles, and they shift from lower to higher 2θ angle as the lattice constant of the substrate increases, indicating that the out-of-plane lattice constant (a_{op}) changes by the epitaxial strains. The rocking curve (not shown) width is less than 0.1° for all the films, also indicating high orientation and crystallinity. Epitaxial relationships

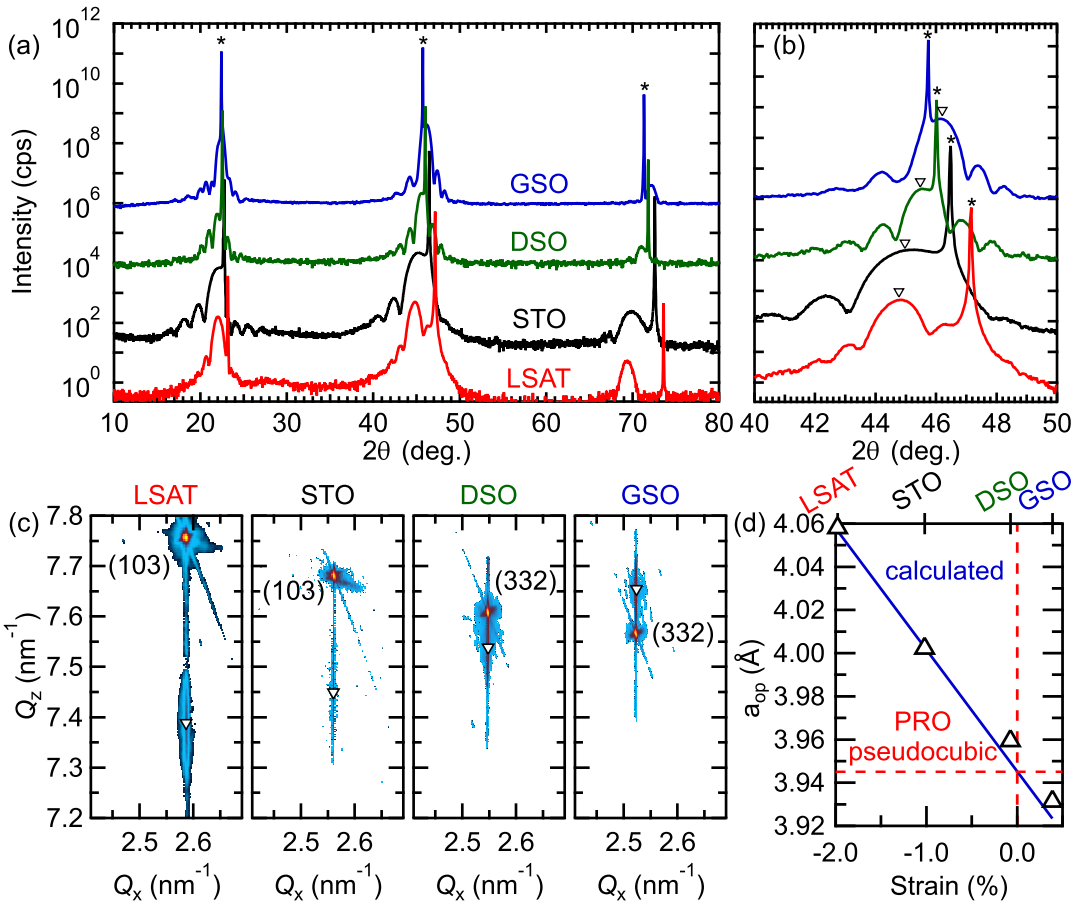

FIG. 2. (a) X-ray diffraction (XRD) 2θ-ω scans and (b) magnified data around the (002) (pseudocubic setting) peak of $PbRuO_3$ films on different substrates. The peaks of substrates and $PbRuO_3$ films are denoted by stars and triangles, respectively. (c) Reciprocal space maps (RSM) for $PbRuO_3$ films around (103) peak of LSAT and STO substrates, and around (332) peak of DSO and GSO substrates. $PbRuO_3$ films peaks are denoted by triangles. (d) Out-of-plane lattice constant (a_{op}) for $PbRuO_3$ films on different substrates. The dashed red lines represent the pseudocubic lattice constants for bulk $PbRuO_3$. The blue line represents the strained a_{op} of $PbRuO_3$ films estimated from a Young's modulus of 0.41.

between the substrates and $PbRuO_3$ films are also clarified by reciprocal space mappings presented in Fig. 2(c), where in-plane lattice constants of $PbRuO_3$ match up with those of all the substrates. These results are summarized in Fig. 2(d). The theoretical line for a_{op} of strained $PbRuO_3$ films can also be calculated from Young's modulus as shown in Fig. 2(d), by assuming fully strained situation, where the Possion's ratio $\nu \approx 0.41$ is deduced as a fitting parameter.

In order to elucidate the strain effect on the electronic phase of $PbRuO_3$, electrical transport measurements were performed. For these measurements, films were processed to Hall-bar structure with a standard photolithography technique especially to acquire precise ρ_H with less intermixing from ρ_{xx}; Hall-bar structure was fabricated by Ar ion milling, and then Ni (10 nm)/Au (50 nm) electrode was attached by electron beam evaporation [Fig. 3(a)]. Because Ar ion-milling process introduces oxygen vacancies to STO substrate and makes it conducting, we will discuss magnetotransport properties of $PbRuO_3$ on LSAT, DSO, and GSO substrates, hereafter.

Temperature dependence of ρ_{xx} is presented in Fig. 3(b). At room temperature, ρ_{xx} of all the films is almost in the same order of magnitude (10^{-4} Ω cm), which is consistent with the previous report for high-pressure synthesized bulk samples [13–15]. ρ_{xx} show metallic temperature dependence down to 2 K with residual resistivity ratio (RRR $\equiv \rho_{xx}(300\text{ K})/\rho_{xx}(2\text{ K})$) of $\approx$1.5, indicating that the RRR of our films are lower than those of bulk samples. Different from previous literature data by both groups, our films do not exhibit an obvious signature of transition at around 90 K as shown in the temperature derivative of ρ_{xx} [Fig. 3(c)]. Temperature hysteresis of ρ_{xx} is also carefully checked around 90 K but not detected, either. This apparent absence of the phase transition can be explained by the epitaxial strain because the transition is concomitant with structural transition. The lower RRR may also be attributed to the strain effect because the reduction of RRR has been reported for the bulk sample as applying statistic pressure [13–15].

Magnetic field (B) dependence of magnetoresistance ratio (MRR(%) $\equiv [\rho_{xx}(B)/\rho_{xx}(0) - 1] \times 100$) obtained at various temperatures are presented in Fig. 4(a). All the films exhibit a slight positive magnetoresistance (MR) at lower temperatures, 0.3–0.6% at 2 K under $B = 9$ T. The intriguing feature here is the deviation from conventional quadratic ($\sim B^2$) positive MR, which is clearly seen for $PbRuO_3$ on DSO and GSO. One explanation can be given by considering a competition between

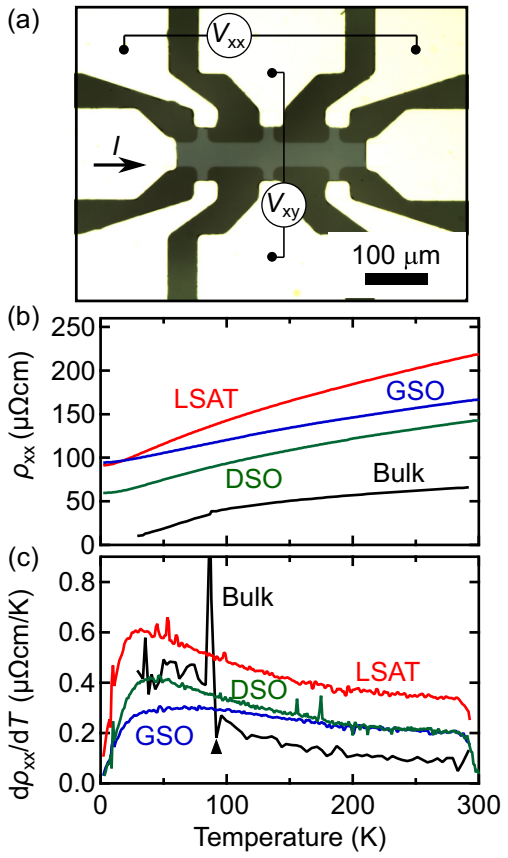

FIG. 3. (a) Device structure for magnetotransport measurements. (b) Temperature dependence of longitudinal resistivity ρ_{xx} and (c) its temperature derivative for $PbRuO_3$ films grown on the different substrates. The bulk data are from Ref. [13]. The triangle indicates the transition temperature of the bulk sample.

the positive quadratic MR and negative MR from spin canting which will be enhanced by magnetic field. Another possible reason is weak antilocalization (WAL) effect, which comes from quantum interference of scattered electrons through spin-orbit coupling (SOC) [19,20]. Although WAL effect has been recently well established in magnetotransport properties in topological materials [21,22], it is a generic characteristic of the materials with strong SOC. Indeed, positive MR due to WAL or anisotropic MR has been reported for $SrRuO_3$ owing to relatively large SOC [23]. In $PbRuO_3$, band structure near Fermi level consists of hybridized Pb-6*s* and Ru-4*d* orbitals as suggested by theoretical calculations [12,14], thus heavy Pb atom may enhance SOC and lead to the observed nonquadratic MR.

As temperature goes up, MRR becomes smaller, changes its sign, and shows bottom, where negative MR becomes maximum, before it becomes negligibly small at around 100 K as shown in Fig. 4(b). This transition in MR can be understood by considering the AFM spin fluctuation previously reported [12,13], which occurs concomitant with the structural transition at 90 K ($= T_{sf}$). At lower temperatures, spin fluctuation is suppressed and positive MR is dominant. With increasing temperature, spin fluctuation is thermally activated more, thus applied magnetic fields yield negative MR by suppressing the magnetic scattering on conduction electrons. Therefore, the change of the bottom position can be interpreted as the change of T_{sf}. T_{sf} has been reported to become lower under hydrostatic pressure for polycrystalline $PbRuO_3$ [13]. Interestingly in Fig. 4(b), the bottom position of most strained $PbRuO_3$ on LSAT substrate is remarkably lower than those of others. Although epitaxial strain is not equivalent with static pressure, we can speculate the observed shift in the bottom position results from the suppression in T_{sf}.

Now we discuss Hall effect, which can detect the magnetic properties because conduction electrons sensitively capture the magnetization in the form of nonlinear Hall effect. Hall resistivity (ρ_H) can generally be written as $\rho_H = R_H B + R_A M + \rho_T$, where the first is ordinarily Hall term with Hall coefficient R_H, the second is anomalous Hall term proportional to magnetization (M) with coefficient R_A, and the third is topological Hall term arising from quantum fictitious magnetic

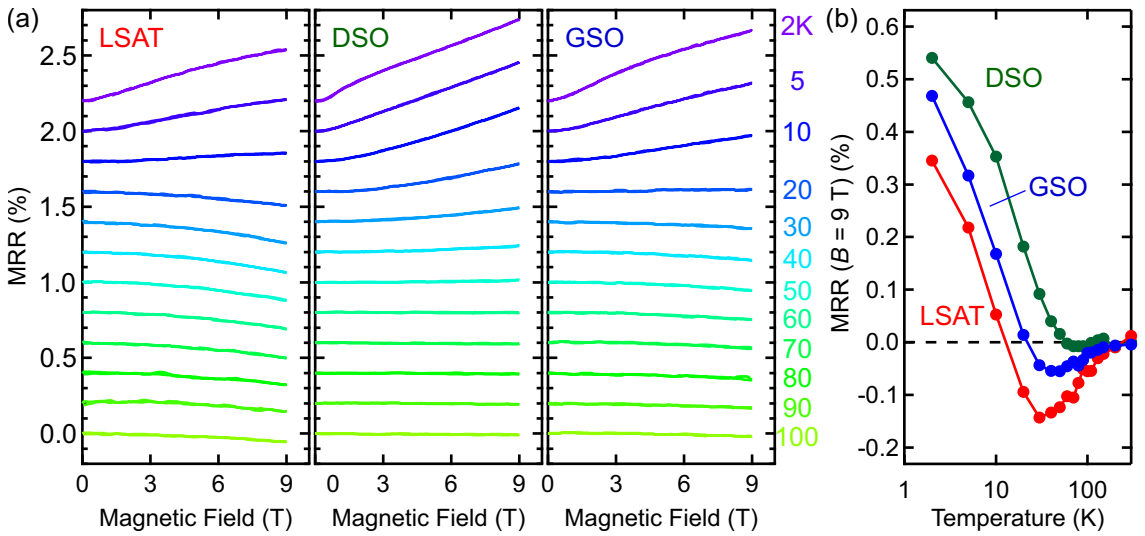

FIG. 4. (a) Magnetic field dependence of the magnetoresistance ratio (MRR) of $PbRuO_3$ films grown on the different substrates. The data are shifted vertically by 0.2% for clarity. (b) Temperature dependence of MRR values at +9 T.

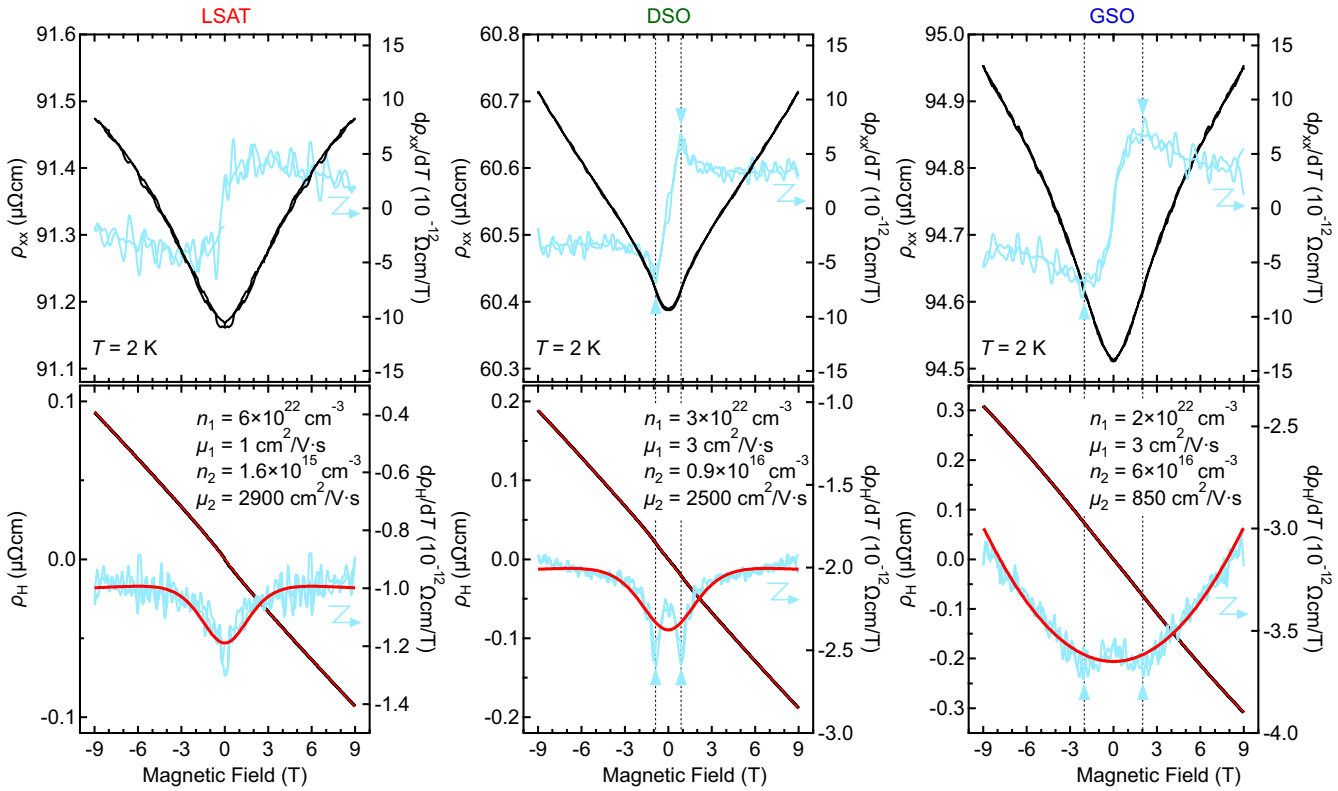

FIG. 5. Magnetic field (B) dependence of (top panels) ρ_{xx} and (bottom panels) $\rho_{\rm H}$ at 2 K for $PbRuO_3$ films grown on the different substrates. Magnetic field derivative is also shown in right axis of each panel. The triangles and the dotted lines indicate the peak position of $d\rho_{xx}/dB$. The solid red lines in the bottom panels are fitted curves using the two-carrier model. Deduced density and mobility of majority (n_1, μ_1) and minority (n_2, μ_2) carriers are indicated.

flux [24,25]. In our films, at higher temperature, $\rho_{\rm H}$ is merely linear to B, but it becomes nonlinear as temperature goes lower. However, we need to carefully consider the multibad effect as an origin of nonlinear Hall effect, which is discussed later.

Figure 5 displays the magnetic field dependence of ρ_{xx} and $\rho_{\rm H}$ and their magnetic field derivative at 2 K for the $PbRuO_3$ films grown on the various substrates. Peak structures are commonly observed in $d\rho_{xx}/dB$ at around 1–2 T, although that of $PbRuO_3$ on LSAT is broader than those of others. This indicates that, at lower temperature, ρ_{xx} deviates from quadratic behavior which is expected for MR originating from Lorentz force as we already discussed. As for $\rho_{\rm H}$, the raw data hardly exhibit nonlinearity as shown in the bottom panels. However, by taking derivatives ($d\rho_{\rm H}/dB$), nonlinear Hall effect has been clearly seen. Intriguingly, for $PbRuO_3$ on DSO and GSO, peak structures appear and their positions match with those of $d\rho_{xx}/dB$, which cannot be explained only by multiband effect and is suggestive of some contribution from magnetic spins, namely, anomalous Hall effect. On the other hand, different from the case of conventional anomalous Hall effect in ferromagnets, $d\rho_{\rm H}/dB$ is not fully saturated even at 9 T. This can be explained by two possibilities: (i) nonlinearity comes from anomalous Hall effect, and because of the antiferromagnetic spin fluctuation, much higher magnetic field is demanded for complete saturation, (ii) nonlinearity does not come from anomalous Hall effect but from multiband effect. Considering the properties of $PbRuO_3$, it is challenging to clearly distinguish these two origins.

Finally, we have attempted to fit the $\rho_{\rm H}(B)$ data by conventional two-carrier model written as below to estimate the multiband effect; $\rho_{\rm H}(B) = [(\mu_1^2 n_1 + \mu_2^2 n_2) + (\mu_1\mu_2 B)^2(n_1 + n_2)]B/e[(\mu_1|n_1| + \mu_2|n_2|)^2 + (\mu_1\mu_2 B)^2(n_1 + n_2)^2]$, where $n_{\rm i}$ and $\mu_{\rm i}$ denote density and mobility for each carrier, respectively. Based on this equation, we have fitted the $\rho_{\rm H}(B)$ data with the constraint of $\rho_{xx}(0) = 1/e(n_1\mu_1 + n_2\mu_2)$. The observed nonlinearity of $\rho_{\rm H}$, including overall trend of $d\rho_{\rm H}/dB$, are well captured by the fitted curves in Fig. 5 considering two types of electrons. However, the fitted curves fail to reproduce the characteristic peaks observed in $PbRuO_3$ on DSO and GSO, indicating that the peak structures do not originate from multiband effect. Moreover, in order to fit the $\rho_{\rm H}(B)$ data, we need to assume the existence of minority carrier with quite high mobility, as high as $\approx$1000 $\rm cm^2/V\,s$, which is unphysical for such complex oxides. We have performed the same fitting for $\rho_{\rm H}(B)$ data obtained at 5 and 10 K, and confirmed the overall trend is well reproduced, although the peaks diminish rapidly at higher temperatures. (See Supplemental Material in Ref. [26] for detail). From these reasons, we can fairly postulate that some magnetic transition occurs in our $PbRuO_3$ films at lower temperature and anomalous Hall effect emerges under applied magnetic fields. Yet, further investigation for magnetization is required to unveil this issue.

In conclusion, high-pressure phase of perovskite $PbRuO_3$ has been successfully synthesized as single crystalline thin films on various substrates with different epitaxial strains by PLD. Opposed to previous studies for bulk polycrystalline samples of $PbRuO_3$ grown under high pressure, clear transition has not been observed in ρ_{xx} on cooling temperature possibly because of the suppression of the structural transition by the epitaxial strains. Magnetotransport measurements clarify the strain effect on the electronic state of $PbRuO_3$, and suppression of AFM spin fluctuation is implicated by magnetoresistance, which is consistent with the reported pressure induced transition for bulk samples. Nonlinear Hall effect is also observed, which is presumably due to anomalous Hall effect emerging from AFM spins. Our present work will be supported by further studies especially in terms of magnetism to clarify the intriguing properties of this unusual perovskite ruthenate.

This work was supported by the Japan Science and Technology Agency Core Research for Evolutional Science and Technology (JST CREST) (No. JPMJCR16F1).

[1] Y. Tokura, Rep. Prog. Phys. **69**, 797 (2006).
[2] K. F. Wang, J. M. Liu, and Z. F. Ren, Adv. Phys. **58**, 321 (2009).
[3] H. Y. Hwang, Y. Iwasa, M. Kawasaki, B. Keimer, N. Nagaosa, and Y. Tokura, Nat. Mater. **11**, 103 (2012).
[4] J. M. Longo, P. M. Raccah, and J. B. Goodenough, J. Appl. Phys. **39**, 1327 (1968).
[5] D. J. Singh, J. Appl. Phys. **79**, 4818 (1996).
[6] I. I. Mazin and D. J. Singh, Phys. Rev. B **56**, 2556 (1997).
[7] C. Q. Jin, J. S. Zhou, J. B. Goodenough, Q. Q. Liu, J. G. Zhao, L. X. Yang, Y. Yu, R. C. Yu, T. Katsura, A. Shatskiy, and E. Ito, Proc. Natl. Acad. Sci. USA **105**, 7115 (2008).
[8] L. Klein, L. Antognazza, T. H. Geballe, M. R. Beasley, and A. Kapitulnik, Phys. Rev. B **60**, 1448 (1999).
[9] J. B. Torrance, P. Lacorre, A. I. Nazzal, E. J. Ansaldo, and C. Niedermayer, Phys. Rev. B **45**, 8209(R) (1992).
[10] J. G. Cheng, J. S. Zhou, J. B. Goodenough, and C. Q. Jin, Phys. Rev. B **85**, 184430 (2012).
[11] J. A. Kafalas and J. M. Longo, Mater. Res. Bull. **5**, 193 (1970).
[12] S. A. J. Kimber, J. A. Rodgers, H. Wu, C. A. Murray, D. N. Argyriou, A. N. Fitch, D. I. Khomskii, and J. P. Attfield, Phys. Rev. Lett. **102**, 046409 (2009).
[13] J. G. Cheng, J. S. Zhou, and J. B. Goodenough, Phys. Rev. B **80**, 174426 (2009).
[14] J. G. Cheng, K. E. Kweon, J. S. Zhou, J. A. Alonso, P. P. Kong, Y. Liu, C. Jin, J. Wu, J. F. Lin, S. A. Larregola, W. Yang, G. Shen, A. H. MacDonald, A. Manthiram, G. S. Hwang, and J. B. Goodenough, Proc. Natl. Acad. Sci. USA **110**, 20003 (2013).
[15] A. F. Kusmartseva, A. Sinclair, J. A. Rodgers, S. A. J. Kimber, and J. P. Attfield, Phys. Rev. B **87**, 165130 (2013).
[16] A. Radetinac, J. Zimmermann, K. Hoyer, H. Zhang, P. Komissinskiy, and L. Alff, J. Appl. Phys. **119**, 055302 (2016).
[17] Y. Kozuka, H. Seki, T. C. Fujita, S. Chakraverty, K. Yoshimatsu, H. Kumigashira, M. Oshima, M. S. Bahramy, R. Arita, and M. Kawasaki, Chem. Mater. **24**, 3746 (2012).
[18] T. C. Fujita, Y. Kozuka, H. Seki, and M. Kawasaki, Phys. Rev. B **87**, 205402 (2013).
[19] S. Hikami, A. I. Larkin, and Y. Nagaoka, Prog. Theor. Phys. **63**, 707 (1980).
[20] J. J. Lin and J. P. Bird, J. Phys.: Condens. Matter **14**, R501 (2002).
[21] M. Z. Hasan and C. L. Kane, Rev. Mod. Phys. **82**, 3045 (2010).
[22] X. L. Qi and S. C. Zhang, Rev. Mod. Phys. **83**, 1057 (2011).
[23] R. Gunnarsson, Phys. Rev. B **85**, 235409 (2012).
[24] N. Nagaosa, J. Sinova, S. Onoda, A. H. MacDonald, and N. P. Ong, Rev. Mod. Phys. **82**, 1539 (2010).
[25] J. Sinova, S. O. Valenzuela, J. Wunderlich, C. H. Back, and T. Jungwirth, Rev. Mod. Phys. **87**, 1213 (2015).
[26] See Supplemental Material at http://link.aps.org/supplemental/10.1103/PhysRevMaterials.4.031401 for an analysis on nonlinear Hall effect at higher temperatures.